Impact of methyl-esterification on the microstructure of calcium-induced polygalacturonic acid gels

Mikaela Börjesson, Giovanni Tizzanini, Anna Ström, Adrien Lerbret, Fabrice Cousin, Ali Assifaoui

Carbohydrate Polymers 370 (2025) 124301

Contents lists available at ScienceDirect

Carbohydrate Polymers

journal homepage: www.elsevier.com/locate/carbpol

Impact of methyl-esterification on the microstructure of calcium-induced polygalacturonic acid gels

Mikaela Börjesson [a,b,c], Giovanni Tizzanini [b], Anna Ström [b], Adrien Lerbret [c,*], Fabrice Cousin [a,*], Ali Assifaoui [c,*]

[a] Laboratoire Léon Brillouin, CEA-Saclay, 91191 Gif-sur-Yvette, France
[b] Department of Chemistry and Chemical Engineering, Chalmers University of Technology, SE-412 96 Göteborg, Sweden
[c] Université Bourgogne Europe, L'Institut Agro, INRAE, UMR PAM, 21000, Dijon, France

ARTICLE INFO

Keywords:
Ionotropic gelation
Polymer network
Mesh size
Hydrogels

ABSTRACT

We investigated the influence of the partial methyl-esterification of polygalacturonic acid (PGA) chains on the structure of ionotropic hydrogels prepared with an external gelation protocol using calcium as the crosslinker and PGA chains with degrees of methylation (DM) of 0, 3, 18, and 34 %. Molar mass determination, viscosity, and small-angle neutron scattering measurements revealed that the methyl-esterification reaction employed reduces the molar mass (M_w) and the intrinsic viscosity, of the PGA chains and increases their overlap concentration, and their persistence length as DM increases. Moreover, the methylation induces turbidity in Ca-PGA hydrogels, which reflects the emergence of mesoscopic heterogeneities, reduces the gradients in PGA and calcium concentrations, as well as in Young's modulus and increases the mesh size of the hydrogels. Complementary molecular dynamics simulations also showed that methylation promotes 3_1 helical conformations of PGA chains and reduces the length of junction zones between cross-linked PGA chains in the presence of calcium. Such effects likely originate from the presence of methyl-ester groups, which decreases the negative charge of methylated PGA chains, weakens their affinity for calcium, and promotes irregular association patterns.

1. Introduction

Polymer-based hydrogels are versatile three-dimensional network materials employed in applications ranging from tissue engineering to drug delivery, and derive their functional diversity from complex structural characteristics (Li & Mooney, 2016; Li & Su, 2018). These hydrogels are composed of interconnected polymer chains that are cross-linked either physically or chemically. They have the capacity to absorb and retain significant amounts of water (typically 90–99 %) while preserving their structural integrity. Recent research underscores the critical role of mesh size and heterogeneities within hydrogel networks in defining their properties and performance. Rose et al. revealed that nanoscale heterogeneities in tetra-PEG hydrogels substantially modify nanoparticle dynamics, crucial for optimizing transport properties in drug delivery systems (Rose et al., 2022). Furthermore, studies demonstrate that introducing connectivity defects within peptide amphiphile and polymer networks profoundly affects rheological behavior, diffusivity, and mechanical properties, illustrating how strategic defect engineering can tailor hydrogel properties such as diffusivity and softness (Matsumoto et al., 2017; Nicolella et al., 2022).

Heterogeneities in hydrogels can originate from irregularities in the polymer network structure, including missing cross-links, chain entanglements, or non-uniform distribution of polymer chains. These structural imperfections lead to varying cross-link densities, resulting in spatial heterogeneity (Jangizehi et al., 2020). Consequently, regions with higher polymer density or fewer defects (resulting in a smaller mesh size) may more effectively restrict drug diffusion than those with lower density or more defects. The diffusion rate depends on whether the drug size matches the network mesh size, determining whether diffusion is fast, slow, or hindered (Li & Mooney, 2016; Maire du Poset, Börjesson, et al., 2020; Rehmann et al., 2017).

Heterogeneities can also arise from the gelation process and the nature of cross-links. Indeed, the gelation of negatively charged polysaccharides such as pectin or alginate involves interactions between divalent cations (crosslinkers) and carboxylate groups of the polymer. As divalent cations diffuse from an external reservoir to the

* Corresponding authors.
E-mail addresses: adrien.lerbret@institut-agro.fr (A. Lerbret), fabrice.cousin@cea.fr (F. Cousin), ali.assifaoui@ube.fr (A. Assifaoui).

https://doi.org/10.1016/j.carbpol.2025.124301
Received 9 February 2025; Received in revised form 20 August 2025; Accepted 26 August 2025
Available online 29 August 2025

polysaccharide solution, the resulting gel exhibits anisotropy with gradients in polymer concentration and macroscopic pores (Caccavo et al., 2016; Schuster et al., 2013; Skjåk-Bræk et al., 1989; Thiele & Hallich, 1957; Thu et al., 2000). Contraction of the gel occurs as polysaccharide chains interact with divalent cations, promoting diffusion of polymer chains close to the gelation front and contributing to the observed heterogeneities (Huynh, Chambin, Maire du Poset, & Assifaoui, 2018; Maki et al., 2011; Wu et al., 2014).

Polygalacturonic acid (PGA) is a linear polysaccharide primarily made up of homogalacturonan (HG) regions, which consist of repeating galacturonic acid (GalA) units. HG regions correspond to the smooth part of pectin, a natural polymer found in the plant cell walls. HG is a significant component of pectin interspersed with branched structures such as rhamnogalacturonan-I (RG-I) and xylogalacturonan (XG) (Assifaoui et al., 2024). These additional domains contribute to the complexity of pectin in comparison to PGA.

In a previous work, we investigated the influence of three divalent cations (Ca^{2+}, Zn^{2+}, Fe^{2+}) on the structure and mechanical properties of ionotropic polygalacturonate (PGA) hydrogels formed via external gelation (Maire du Poset et al., 2018; Maire du Poset et al., 2019). Our findings showed that early-stage hydrogels exhibit homogeneous regions with consistent mesh sizes (75 ± 5 Å) across all the studied divalent cations. The similarity of the mesh size with the persistence length of PGA (Lp = 70 Å) suggests that the polymer chains restrict the network contraction to a mesh size approximately equal to their Lp, beyond which further contraction is limited (Maire du Poset, Börjesson, et al., 2020). However, in later stages of gel formation, differences in mechanical properties, turbidity, and local structure are observed. In the case of Ca(II)-PGA hydrogels, the mesh size increases continuously all along the gel to account for the polymer concentration gradient, so that hydrogels maintain a homogeneous structure. Conversely, the mesh size remains constant at a local scale in Zn(II)-PGA and Fe(II)-PGA hydrogels, which induces the formation of mesoscopic heterogeneities to account for the polymer concentration gradient. These structural differences are attributed to the coordination mode between the cations and the galacturonic acid (GalA) unit. This results in a stronger association for zinc and iron, where the coordination is primarily monodentate, compared to calcium, where the coordination is preferentially bidentate. (Huynh et al., 2016; Lerbret & Assifaoui, 2022; Maire du Poset, Zitolo, Cousin, Assifaoui, & Lerbret, 2020). The mechanism of polyuronates gelation induced by divalent cations follows two successive steps: (i) the diffusion of divalent cations induces the formation of monocomplexes and some point-like cross-links (GalA-Ca-GalA ionic bridges), and then (ii) the increase in calcium amount leads to the formation of lateral associations between GalA chains (Cao et al., 2020).

This study investigates the influence of partial methyl-esterification of PGA (MeO-PGA) chains on the local structure of anisotropic calcium-based hydrogels (Ca-MeO-PGA). Four degrees of methylation (DM) were considered: 0 %, 3 %, 18 %, and 34 %. Calcium ions were selected as the cross-linking agents due to their ability to form homogeneous hydrogels with tunable mesh sizes at the local scale (Maire du Poset et al., 2019). The study examined the viscosity and molar mass distribution of polymer solutions as a function of DM. Molecular dynamics (MD) simulations were conducted to explore the behavior of GalA chains at DM levels of 0 % and 31 %, as well as their interactions with calcium ions. Additionally, small-angle neutron scattering (SANS) was employed to characterize the local structure of MeO-PGA solutions at various DMs, and the resulting hydrogels were examined in detail. Together, these complementary techniques provide a detailed and comprehensive understanding of how methyl-esterification of PGA modulates the structural and functional properties of hydrogel networks.

2. Material and methods

2.1. Materials

Polygalacturonic acid (PGA) from oranges (CAS number: 25990-10-7, purity ≥ 90 %), sodium chloride (purity ≥ 99 %), calcium chloride dihydrate (purity ≥ 99 %), NaOH (purity ≥ 98 %), $NaNO_3$ (purity ≥ 99 %), D_2O (99.9 atom % D), and sodium 3-(trimethylsilyl)-1-propanesulfonate (DSS) were purchased from Sigma (St. Louis, MO, USA). Absolute methanol and absolute ethanol were purchased from VWR (HPLC-grade, purity > 99.7 %).

2.2. Methyl-esterification of polygalacturonic acid (PGA)

Methyl-esterification of polygalacturonic acid (PGA) involves a reaction between the carboxylic groups of GalA and methanol, which occurs at low temperatures in an acidic environment with acetyl chloride as a catalyst. As the reaction takes place under heterogeneous conditions, the distribution of methyl groups is likely not random but rather arranged in blocks. Briefly, a cooled methanol solution (200 mL) is added slowly to an acetyl chloride solution (10 mL) and stirred for 1 h (Rosenbohm, Lundt, Christensen, & Young, 2003). Then, 3 g of polygalacturonic acid is added to this solution and stirred in a closed flask in a cold chamber at 8 ± 1 °C for various durations (1, 5 or 10 days). After each duration, the partially methyl-esterified PGA (MeO-PGA) is filtered and washed first with 60 % aqueous ethanol acidified with HCl, then with absolute ethanol. The MeO-PGA is then dried at room temperature under vacuum. Methylation of polysaccharides is known to degrade the polymer (Chen et al., 2015; Rosenbohm, Lundt, Christensen, & Young, 2003). The degree of methyl-esterification (DM) of the obtained powders was evaluated by Nuclear Magnetic Resonance (NMR), as described below.

2.3. Preparation of solutions and gels

The obtained powder (PGA or MeO-PGA) was dispersed in a 10 mM sodium chloride solution and stirred for 2 h. To ensure solubilization and conversion of galacturonic acid to sodium galacturonate, the pH was adjusted to 5.5 (2 units higher than the pKa of PGA) using a sodium hydroxide solution. The resulting solution was then dialyzed three times against 10 mM NaCl for 2 h using a dialysis membrane with a molecular weight cutoff of 3.5 kDa, maintaining a volume ratio of 1:10 between the polymer solution and the dialysis bath. The calcium solution was prepared by dissolving a specific amount of $CaCl_2{\cdot}2H_2O$ in a 10 mM sodium chloride solution to achieve a final concentration of 100 mM.

Hydrogels were prepared by using the protocol described in our previous study (Fig. S1).(Maire du Poset et al., 2018) Briefly, we poured 5 mL of the PGA or MeO-PGA solution (20 $g.L^{-1}$) in a glass tube (diameter 2.1 cm). The lower part of the glass tube, on which a dialysis membrane was set to separate the solution from the reservoir, was immersed into a 50 mL reservoir of a calcium solution (100 mM) for 24 h to ensure that the gels were fully formed. The setup was covered during the gelation process with paraffin film to limit the evaporation of water. The obtained gels were cut into slices corresponding to different distances z to the dialysis membrane. The exact thickness of a given slice was systematically measured after the cut. Slice 1 refers to the gel slice nearest to the dialysis membrane (near part), while slice 4 refers to the gel slice farthest from the dialysis membrane (far part). For small angle neutron scattering (SANS) measurements (see below), the same protocol was applied to both the PGA solution and hydrogels, except that H_2O was replaced by D_2O.

2.4. Physical-chemical characterizations

2.4.1. Determination of Degree of Methyl-esterification (DM) by NMR

DM of PGA and methylated PGA was determined using ^1H NMR,

following the protocol presented by Müller-Maatsch and co-workers (Müller-Maatsch et al., 2014). The samples (1 mg/mL) were incubated for 2 h at room temperature with 1 mL of 0.4 M NaOH in D_2O containing 8 mM of DSS as internal standard. The supernatant was centrifuged, filtered (Corning, NY, 0.2 μm, Germany), and transferred to NMR tubes. ^1H NMR spectra were acquired on an Avance 600 MHz spectrometer (Bruker Avance III, Violet system, USA), equipped with a triple-resonance inverse cryoprobe ($^1H/^{13}C/^{15}N$, QCI) with *Z*-gradient capabilities. The spectrometer operated at 599.75 MHz for proton detection. Spectra were collected at 298 K, with 32 K complex points, using a 90° pulse length. Sixty-four scans were acquired with a spectral width of 11,905 Hz, an acquisition time of 2.06, and a relaxation delay (d1) of 2 s. ^1H NMR spectra were acquired with water suppression and were processed with MestReC software. The quantitative determination of methanol was obtained by manual integration of its corresponding signal at 3.34 ppm and comparison with the area of the DSS peak (Rosenbohm, Lundt, Christensen, & Young, 2003). Integrals were converted into mass value (mg) according to Eq. (1).

$$A_{CH_3OH} \times \frac{EW_{CH_3OH}}{mg_{CH_3OH}} = A_{DSS} \times \frac{EW_{DSS}}{mg_{DSS}} \quad (1)$$

where A_{CH3OH} is the spectral area of methanol, A_{DSS} is the spectral area of the internal standard, EW_{CH3OH} is the equivalent weight of methanol, and EW_{DSS} is the equivalent weight of the internal standard; EW is the fraction of the analyte molecular weight and the number of hydrogens in the analyte's signal. Through the content of MeOH and the content of GalA, the DM was calculated according to Eq. (2).

$$Degree\ of\ methylation = \frac{mol\ of\ methanol}{mol\ of\ galacturonic\ acid} \times 100\,(\%) \quad (2)$$

2.5. Molar mass determination using size exclusion chromatography

SEC-MALS-IV was employed to determine the molar mass (M_n and M_W) of the PGA and MeO-PGA samples. An aqueous solvent with 20 mM of $NaNO_3$ and 0.002 % *w*/w NaN_3 was used as a mobile phase. The eluent was filtered (0.22 μm MCE membrane filters, MF-Millipore™, Merck) and degassed through sonication prior use. The samples were wetted with EtOH for 30 min, then dispersed in a solvent with the same composition as the eluent over 4 h. The samples were neutralized to pH 7 with a few μL of a solution of 0.1 M NaOH, then left stirring overnight at room temperature. The solutions were heated for 10 min at 80 °C.

The PGA and the MeO-PGA samples of 1 mg/mL were filtered through a syringe filter (Acrodisc 13 mm minispike with 0.45 μm water wettable PTFE) and injected in a TSKgel $GMPW_{XL}$ 7.8 × 300 mm column Tosoh with a particle size of 13 μm. The flow rate used was 0.5 mL/min and the total injection volume was 100 μL.

The HPLC system consists of a degasser (1260 Infinity II Degasser by Agilent), a pump system (1260 Infinity II Quaternary Pump by Agilent), and an autoinjector (1260 Infinity II Vialsampler by Agilent). One inline filter (Millipore VM 0.05 μm filter) and a TSKgel guard column PW_{XL} 6.0 × 40 mm with a particle size of 12 μm placed before the column. Three detectors were used for the analysis: a DAWN HELEOS-II multiangle laser light scattering detector, a Viscostar 3 viscometer (viscometric detector), and an Optilab rEX refractive index detector. The data was analyzed using the software ASTRA (version 7.3.2). The dn/dc used in the analysis was 0.1460 mL/g for all the samples (Kpodo et al., 2017). Three replicates per sample were run and analyzed. Results are reported as average values and standard deviation (SD).

2.6. Viscosity measurements

The viscosity measurements of polymer solutions were performed on an Anton Paar Modular Compact Rheometer MCR 302. A sandblasted plate–plate geometry with a diameter of 50 mm was used with 1 mm gap. The temperature was fixed to 22 °C using a VISCOTHERM VT2 water bath from Anton Paar. A shear rate sweep was performed between 1 and 50 s^{-1}. The overlap concentration (C*) was determined graphically by plotting the viscosity of PGA and MeO-PGA solutions as a function of concentration (5 to 20 $g.L^{-1}$). The viscosity for the C* comparison was taken at 20 s^{-1}.

2.7. Young Modulus determination

The Young's modulus of Ca-PGA and Ca-MeO-PGA hydrogels was measured using a CT3 Texturometer (Brookfield) equipped with a 25 mm diameter plate geometry and a 1.5 kg load cell. To evaluate the variation in rigidity along the gel length, each slice was analyzed individually. Measurements were performed at room temperature and immediately after gel formation to prevent drying and syneresis. A 40 % compression strain was applied at a constant probe speed of 0.5 mm/s. Each measurement was carried out in triplicate. The Young's modulus (E) was determined by applying a defined strain (γ) and recording the resulting stress (σ).

2.8. Calcium amount determinations

Each slice of hydrogels was dried in an oven for 24 h at 100 °C. The final total weight (dry matter) corresponds mainly to the quantity of both PGA and cation inside the slice. The calcium content was quantified by inductively coupled plasma atomic emission spectroscopy (ICP-AES) iCAP 7400 (Thermo Scientific, Waltham, MA, USA).

2.9. Small angle neutron scattering (SANS)

SANS measurements were conducted using the PAXY diffractometer instrument at Laboratoire Léon Brillouin (CEA, Saclay, France). Four configurations were employed, using various neutron wavelengths and sample-detector distances (λ = 15 Å, D = 6.7 m; λ = 13 Å, D = 5 m; λ = 8.5 Å, D = 3 m; λ = 5 Å, D = 1 m) to cover the 0.0032–0.5 $Å^{-1}$ scattering vector range. Standard corrections were applied to the raw signal for sample volume, neutron beam transmission, empty cell signal, and detector efficiency to obtain scattering in absolute units. The signal measured from the blank sample (buffer) was then subtracted. D_2O was used instead of H_2O for the solubilization and dialysis of PGA and MeO-PGA, as well as for the gel preparation, to achieve good contrast between the solvent and the polymer network within the gels and to minimize incoherent scattering. After the gelation process, 2 mm thick cylindrical hydrogel slices were placed between two quartz windows separated by a 2 mm spacer, as described in our previous study (Maire du Poset et al., 2018). During measurements, the incoming neutron beam was perpendicular to the faces of the cylinder.

2.10. Molecular dynamics (MD) simulations

We performed molecular dynamics (MD) simulations using the GROMACS package (Abraham et al., 2015; Van Der Spoel et al., 2005) to better understand the influence of partial methyl-esterification on the conformation of PGA chains and on their calcium-induced self-association. Briefly, we first built non-methylated, 16-units long, PGA chains in the 2_1 helical conformation following a procedure described in our previous studies (Assifaoui et al., 2015; Huynh et al., 2016). Then, we methyl-esterified 5 randomly selected GalA units on each $GalA_{16}$ chain, which corresponds to a degree of methylation (DM) of about 31 % (5/16) and is close to the maximum DM obtained experimentally (34 %). However, the random distribution of methyl esters along the PGA chains may not accurately reflect the blockwise distribution (BD) resulting from a heterogeneous reaction under experimental conditions. Simulated systems were composed of either methylated (DM = 31 %) or non-methylated (DM = 0 %) $GalA_{16}$ chains randomly distributed in cubic simulation boxes at [GalA] concentrations of 20 $g.L^{-1}$ and 40 $g.L^{-1}$, which correspond on one hand to the concentration used experimentally

to prepare hydrogels and on the other hand to the concentration determined in the nearest part of hydrogels from the dialysis membrane (Fig. S1). Moreover, $[Ca^{2+}]/[GalA]$ molar ratios, R, of 0.0, 0.25, and 0.5 were considered so as to simulate either GalA solutions ($R = 0.0$) or the association of PGA chains in the presence of calcium following the egg-box model (EBM) (Grant, Morris, Rees, Smith, & Thom, 1973). For each simulated system, three independent initial configurations were built. Sodium or chloride counterions were added to neutralize the total charge of the system, as required for accurate electrostatic calculations using particle mesh ewald summation in molecular dynamics simulations. All simulations were performed at a temperature of 300 K and were run for 500 ns. Calculated properties (helicity parameters of PGA chains, radial distribution functions, junction zone size distributions, etc.) were averaged over the second half (250 ns $\leq t_{sim} \leq$ 500 ns) of three independent simulation trajectories. Further details on these simulations are provided in the supplementary material.

3. Results

3.1. Methyl-esterification of PGA

The NMR spectra of saponified PGA and methyl-esterified PGA are shown in Fig. S2 in the Supporting Information. The degree of methylation (DM) was calculated from NMR measurements, using Eqs. (1) and (2), as proposed by Müller-Maatsch et al. and Rosenbohm et al. (Müller-Maatsch et al., 2014; Rosenbohm, Lundt, Christensen, & Young, 2003). For reaction times of 1, 5, and 10 days, the DM obtained were equal to 3 %, 18 %, and 34 %, respectively. Therefore, the methyl-esterified samples studied were labeled as MeO-PGA-3, MeO-PGA-18, and MeO-PGA-34, corresponding to DM values of 3, 18 and 34 %, respectively.

3.2. Microstructure of PGA and methyl-esterified PGA in solution

SEC-MALS was employed to study the change in the number and weight-averaged molar mass (M_n and M_W, respectively) of the polymers with reaction time.

As shown in Table 1, a decrease in M_w and M_n is observed for the two samples with the highest degrees of methylation (DM), which also correspond to the longest reaction times (5 and 10 days). The M_w of PGA chains with the highest DM has reduced from 110 to 70 kDa. The intrinsic viscosity, as obtained from SEC coupled with a viscometric detector, follows the same trend as M_n and M_w (reduction for the two samples with the highest DM), corroborating the results obtained from the MALS detector. Mass recoveries of the injected volume were 85, 75, 68 and 70 % for PGA, MeO-PGA-3, MeO-PGA-18 and MeO-PGA-34, respectively.

The viscosity of the PGA and MeO-PGA samples were measured as a function of shear rate (1–50 s^{-1}) and polymer concentrations (5–20 g.L^{-1}). All samples showed Newtonian behavior within the range of shear rates tested (Fig. S3), and the dynamic viscosity was plotted as a function of concentration (Fig. 1). The overlap concentration (C*), which represents the threshold concentration at which polymer chains begin to overlap, corresponds to the inflexion point between the two observed linear regimes: the dilute and semi-dilute regimes. C* is similar for PGA and MeO-PGA-3 and close to 11.5 g.L^{-1}. As DM further increases, C* increases to 12.5 and 15.0 g.L^{-1} for MeO-PGA-18 and MeO-PGA-34, respectively. The increase in C* of the methylated PGA samples, as determined using rotational rheology, confirms the observed reduction in molar mass and intrinsic viscosity as observed by molar mass determination using SEC-MALS-IV.

Table 1
Molar mass and intrinsic viscosity ([η]) of PGA and MeO-PGA as obtained from SEC-MALS-IV. M_n stands for the number-averaged molar mass, M_w for the weight-averaged molar mass, $Đ_M$ is the molar-mass dispersity.

Samples	M_n (kDa)	M_w (kDa)	$Đ_M$ (M_n/M_w)	[η] (mL/g)
PGA	43 (± 2)	110 (± 3)	2.6	200 (± 7)
MeO-PGA-3	35 (± 6)	114 (± 5)	3.3	201 (± 6)
MeO-PGA-18	28 (± 9)	85 (± 12)	3.0	170 (± 9)
MeO-PGA-34	27 (± 2)	70 (± 2)	2.6	110 (± 3)

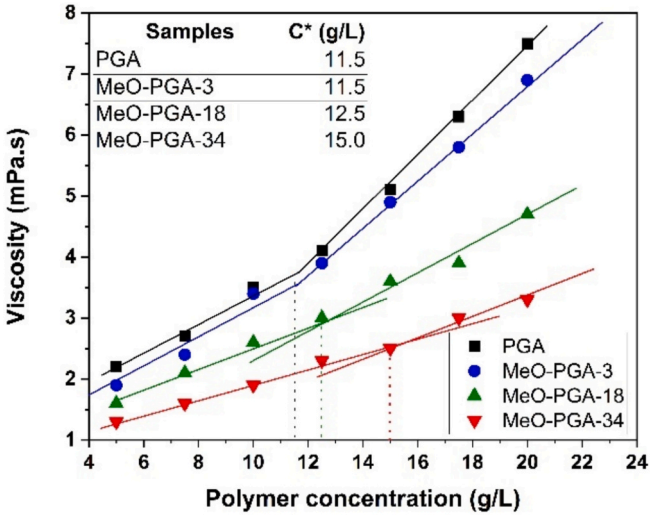

Fig. 1. Viscosity as a function of polymer concentration for PGA and partially methyl-esterified PGA solutions ($T = 22$ °C and pH 5.5).

Small angle neutron scattering (SANS) measurements of PGA, MeO-PGA-3, MeO-PGA-18 and MeO-PGA-34 were performed in 10 mM NaCl solution in deuterated water and at two different polymer concentrations (5 and 20 g.L^{-1}) (Fig. 2 and Fig. S4). For all samples, the spectra exhibit two distinct regimes: a q^{-1} decay at large q and a $q^{-\alpha}$ decay at the lowest q, with the crossover point located at q*. The q^{-1} dependence indicates the rod-like behavior of the polymer at a local scale. The $q^{-\alpha}$ decay indicates the presence of limited aggregation of PGA due to the original batch from the manufacturer. An exponent $\alpha = 2.7$ is observed for PGA, consistent with our previous studies (Maire du Poset et al., 2018; Maire du Poset et al., 2019) and is also found for all methyl-esterified samples, showing that methylation does not induce further

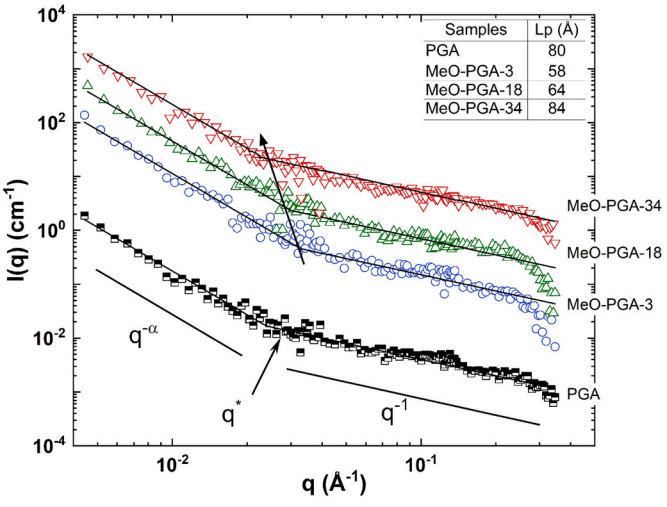

Fig. 2. SANS spectra of PGA and methyl-esterified PGA solutions at a concentration of 5 g.L^{-1}. The solutions were prepared in sodium chloride solution (10 mM), the pH was adjusted to 5.5. The crossover point (q*) decreases with an increase of the DM of PGA chains except for the PGA 0 % sample, as indicated by an arrow. The curves are offset to facilitate the comparison of spectra. The inset provides the Lp values calculated from the following equation: $q^* = 6/(\pi Lp)$.

aggregation. The same decay is observed below C* at low polymer concentration of 5 g.L^{-1} in dilute regime and above C* at 20 g.L^{-1}, indicating that the limited aggregation is not correlated to the polymer concentration. In comparison, Alba et al. found a low-q decay ranging from −1.5 to −2.1 using small-angle X-ray scattering (SAXS) measurements on 100 mM NaCl, pH 7 solutions of pectin with DM ranging from 10 % to 50 %, which were beforehand centrifuged to remove any insoluble material or aggregates (Alba, Bingham, & Kontogiorgos, 2017; Alba et al., 2018). In dilute regime, SANS spectra at 5 g.L^{-1} allows to determine the persistence length Lp of the chains from the crossover between the two regimes at $q^* = 6/(\pi Lp)$. The crossover is shifted to larger q at 20 g.L^{-1} (Fig. S4). Since the polymer concentration is above C*, the mean average distance between neighboring chains may be lower than Lp, which can no longer be determined.

As shown in Fig. 2, PGA in solution exhibits a persistence length (Lp) value close to 80 Å.(Maire du Poset et al., 2018) The sample with the lowest DM showed a significant decrease of Lp down to 58 Å (Fig. 2). As methyl-esterification occurs, an increase of Lp is observed, suggesting that methylation rigidifies the polymer chains (Table 1). The Lp values are 58 Å, 64 Å, and 84 Å for MeO-PGA at degrees of methylation (DM) of 3, 18, and 34 %, respectively. Moreover, the methylation is accompanied by a continuous polymer degradation, as confirmed by a significant reduction in M_w and [η], which explains the shift of C* to higher values for methylated PGA samples subjected to longer reaction times.

3.3. Microstructure of calcium gels made from PGA and methyl-esterified PGA

The protocol designed for the hydrogel formation relies on the use of a solution of PGA chains above C* whatever the DM studied. This indeed allows to obtain hydrogels in all cases. Fig. 3 shows photographs of calcium-based hydrogels at various DM: 0 %, 3 %, 18 % and 34 %. The gel made by PGA is totally transparent, consistent with our previous studies (Maire du Poset et al., 2018; Maire du Poset et al., 2019; Maire du Poset, Börjesson, et al., 2020). Visual inspection of the obtained gels reveals an increase in turbidity with higher DM levels. The observed turbidity remains at a moderate level, as the samples prepared at DM 34 % are still visibly transparent despite their 2 cm thickness. This suggests that the heterogeneities responsible for light scattering are relatively small and likely of similar order of magnitude throughout the gel. This is different from what was observed in Zn(II)-PGA and Fe(II)-PGA hydrogels at DM = 0 % designed with the same protocol, which exhibited a gradient of turbidity along their height, with a nearest part transparent, revealing a progressive growth of heterogeneities from the nearest part to the upper part (Maire du Poset et al., 2018; Maire du Poset et al., 2019).

It was observed that the gel obtained by MeO-PGA-34 appeared softer compared to the other gels. The obtained gels were then cut into 4 slices and the amounts of polymer and total calcium were determined in each slice. The amount of polymer was obtained from SANS measurements thanks to the normalization of the scattering spectra by using the SANS spectra of PGA at 20 g.L^{-1} (Fig. 4). As expected, the concentration of the polymer decreases from slice 1 to slice 4. This decrease is accompanied by a reduction in rigidity of the gel, a well-known phenomenon which is due to the external gelation and observed by various researchers (Huynh, Chambin, Maire du Poset, & Assifaoui, 2018; Maire du Poset et al., 2019; Maki et al., 2011; Mørch et al., 2006; Schuster et al., 2016; Skjåk-Bræk et al., 1989; Thu et al., 2000; Wu et al., 2011). The same tendency is observed for the evolution of the calcium concentration, which decreased from the near part to the furthest part of the gel (Table S2). The molar ratio R (=[Ca^{2+}]/[GalA]) was calculated and is shown in Fig. S5 in the Supporting Information. For high DM (18 % and 34 %), the molar ratio in slices 1 and 2 is lower compared to those of Ca-PGA and Ca-MeO-PGA-3 samples, indicating that fewer calcium ions are required to form a stable gel. Moreover, the reduction in polymer concentration from S1 to S4 is smaller in Ca-MeO-PGA-34 than in other gels (Fig. 4a), suggesting a more uniform distribution of the polymer within the gel. As shown in Fig. 4b, a decrease in Young's modulus from the region nearest the membrane to the furthest part of the gel emerges (Maire du Poset et al., 2018; Maire du Poset et al., 2019; Maire du Poset, Börjesson, et al., 2020), as well as decrease in Young's moduli with increasing DM. It must be noted that the gel MeO-PGA-34 was soft and the slice 3 was too soft for measurement.

3.4. SANS measurements

Gels obtained from PGA and MeO-PGA were cut into 4 slices, which were then measured by SANS. Fig. S6 in the Supporting Information compares for each type of chains the scattering of the different slices with the scattering of the reference solutions of PGA and MeO-PGA chains at 20 g.L^{-1}, i.e. the nominal concentration of chains used to design the gels. In all cases, the scattering curves of the different slices of hydrogels exhibit the same features: (i) at both low and large q values, they superimpose with the scattering of the reference solution, differing only by a scaling factor (k), (ii) at intermediate q values, they exhibit a shoulder that is more or less marked depending on the slice and/or the methylation ratio. This additional shoulder evidences a new correlation length within the cross-linked gel, and is the structural signature of the mesh size of the network (ξ). The fact that this additional term does not modify the structure at the lowest probed q shows that the new correlation due to the cross-linking has been formed within the pre-existing PGA chain structure. The factor k enabling to rescale the low q part of the hydrogel spectrum to that of the reference solution accounts for the change of polymer concentration within the different slices from the reference solution during the gelation process. Its evaluation allows then to obtain the polymer concentration in each slice (Fig. 4). The mesh size ξ can be obtained from the fit of the shoulder by an Ornstein-Zernike (OZ) structure factor, i.e. a Lorentzian function that enables to extract one correlation length.

For each gel, the scattering curves have thus been fitted successfully with the following equation (Eq. (3)):

$$I(q)_{Gel} = k\, I(q)_{solution\_reference} + \beta \frac{1}{1 + (q\xi)^2} \quad (3)$$

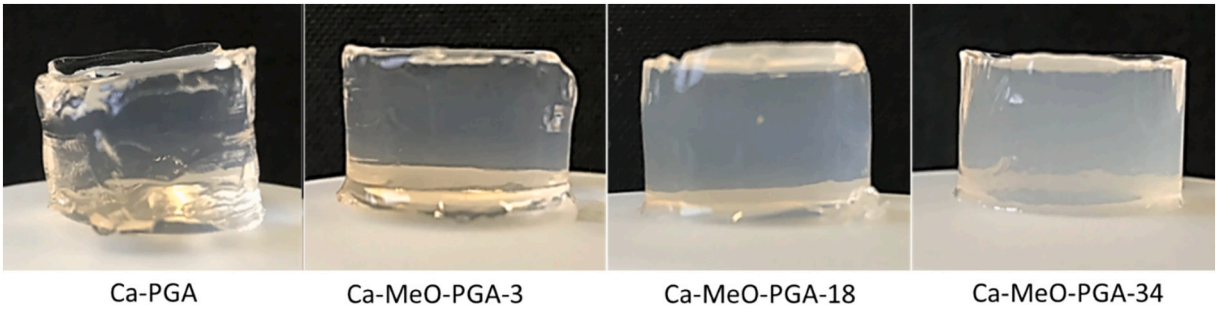

Fig. 3. Photographs of the Ca-PGA hydrogel, and the three partially methyl-esterified PGA (Ca-MeO-PGA) hydrogels considered in this study.

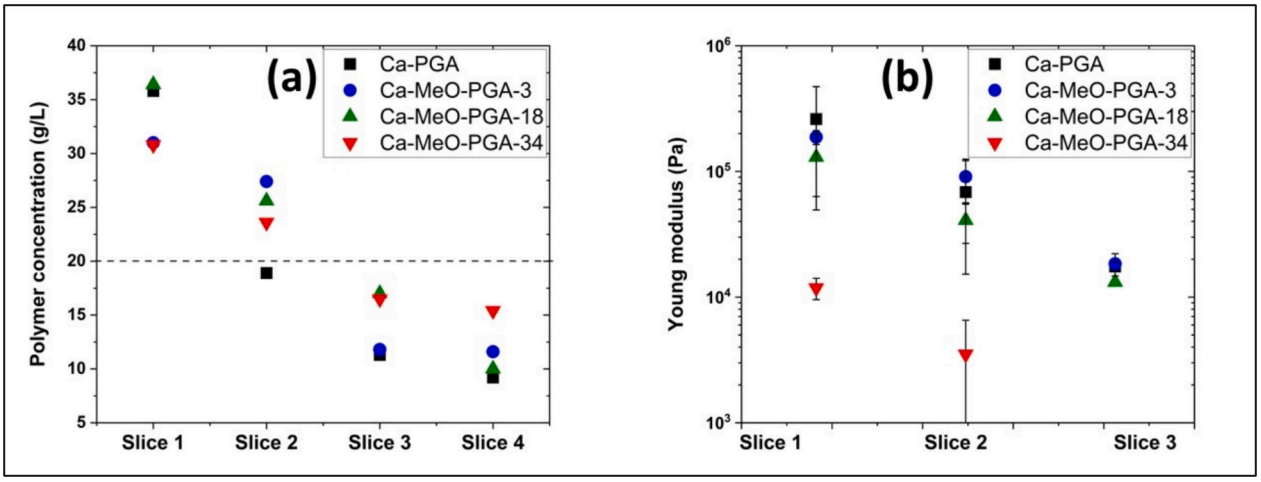

Fig. 4. Evolution of the polymer concentration (a) and the Young modulus (b) in Ca-PGA and Ca-MeO-PGA gels as a function of the slice position along the gel. Slice 1 represents the part of the gel closest to the dialysis membrane, while slice 4 or slice 3 represent the part furthest from the membrane. The concentration of the polymer was determined from the normalization of SANS spectra. The Young modulus of slice 3 of the Ca-MeO-PGA-34 gel could not be determined, because this slice was too soft.

where k is the pre-factor enabling to rescale the concentration of gel to the nominal concentration of solution, ξ is the mesh size of the gel structure and β is a pre-factor.

Fig. 5 shows the scattering of the slice 1 of all samples, along with the scattering of the reference solutions of PGA and MeO-PGA chains at 20 g. L^{-1} and the best fits of data. The respective contributions to these fits of the scattering from the reference solution and from the OZ function are also displayed. The values of the different ξ of slices 1 are reported in Table 2.

The mesh size of the Ca-PGA gel is similar to the Lp of the chains, as observed in our previous work (Maire du Poset et al., 2019), showing that the shrinkage of the forming network in the vicinity of the dialysis

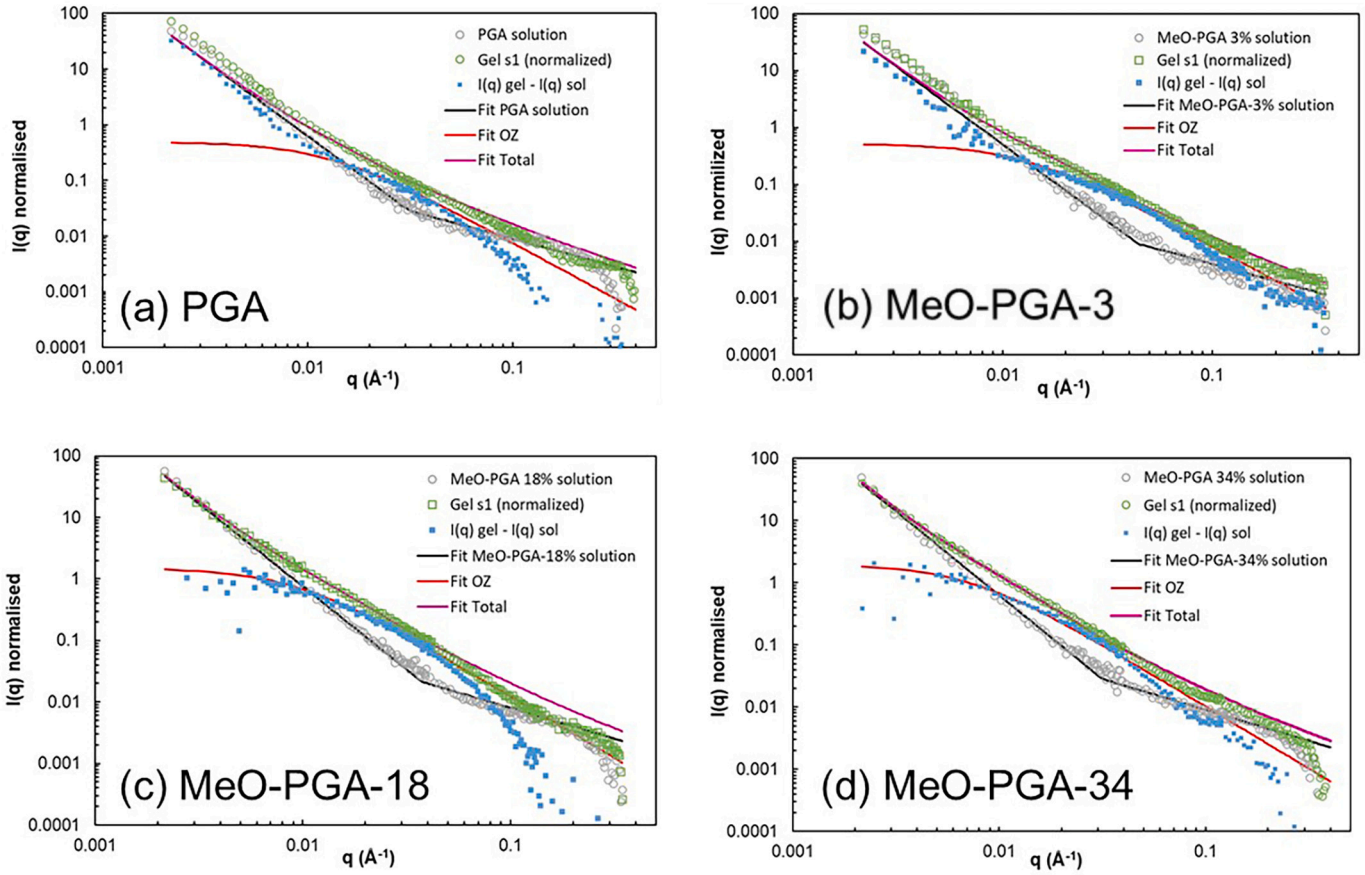

Fig. 5. SANS spectra of the slice 1 from the gels Ca-PGA (a) and Ca-MeO-PGA-DM (DM = 3 (b), 18 (c), 34 (d)) and of their respective reference solutions at 20 g.L^{-1} used to prepare them. The Ornstein-Zernicke (OZ) fitting (red line), the Lorentzian ($I(q)_{gel}$-$I(q)_{sol}$) behavior (blue dots) and the total fit for the gel (purple line) are also shown. (For interpretation of the references to colour in this figure legend, the reader is referred to the web version of this article.)

Table 2
Persistence length (Lp), mesh size (ξ), and ξ/Lp ratio for the various gels measured by SANS. Measurements were conducted in solution for Lp and in gel for ξ.

	DM 0 %	DM 3 %	DM 18 %	DM 34 %
Lp (Å) 5 g.L^{-1}	80	58	64	84
ξ, s1 (Å)	80	80	110	140
ξ/Lp	1.0	1.4	1.7	1.7

membrane is limited by the stiffness of the chains. Conversely, for all the methyl-esterified samples the mesh sizes become larger than the Lp, with a ξ/Lp ratio that progressively increases with DM (1.4 at DM = 3 %, 1.7 at DM = 18 % and 1.7 at DM = 34 %). The crosslinking pattern between calcium ions and PGA chains is probably disrupted when some of the carboxylate groups are substituted with methyl groups (see the following MD simulation results). This partial disruption of calcium-PGA crosslinking interactions caused by methyl-esterification is also evidenced with the progressive increase of the mesh size when increasing DM, from 80 Å at DM = 0 % to 140 Å at DM = 34 %. This increase represents indeed an increase of mesh volume ($\propto \xi^3$) of about a factor 5 although the polymer concentrations remain of the same order of magnitude from one DM to another (Fig. 4).

The progressive shift of the shoulder associated with the mesh toward low q when passing from slice 1 to slice 4 reflects a progressive increase of the mesh size (Fig. S6). This shift toward low q complicates the fit of the shoulder with the OZ function, since it is no longer within the q-range where its scattering dominates that of the initial PGA and PGA-derived solutions. Moreover, the overall scattered intensity decreases with respect to that of slice 1 since the PGA concentration decreases. We have thus decided not to fit the scattering of slices 2 to 4 as errors bars would be large. The progressive increase of the mesh size in hydrogels of pure Ca-PGA hydrogels designed with the same protocol was already reported in (Maire du Poset et al., 2019). It enables to account for the decrease of chain concentration along the gel while keeping locally the structure homogeneous. Remarkably, for the sample with DM = 34 %, the scattering patterns of all slices nearly superimpose (Fig. S6d in the Supporting Information), showing that the mesh size is almost constant throughout the whole hydrogel, a feature consistent with the fact that the concentration of chains weakly varies within such hydrogel (Fig. 4a).

3.5. MD simulations

3.5.1. Chain conformation

We first investigated the influence of methyl-esterification on the conformation of hexadecameric GalA chains, corresponding to PGA with a degree of polymerisation (DP) of 16. For simplicity, we refer to these as "PGA chains" throughout the text. For this purpose, we determined their local helical parameters, namely the helix raise h (also called helix pitch) and the helix turn angle θ (see ref. (Lerbret & Assifaoui, 2022; Perić et al., 2008)) for further definition and calculation details). The probability distributions of the helix raise h are slightly shifted toward larger values upon methyl-esterification, whatever the GalA concentration and the [Ca^{2+}]/[GalA] molar ratio R considered (see Fig. S7 in Supporting Information), so that the mean value of h increases very slightly (from 4.39 Å to 4.40 Å at molar ratios R of 0.0 and 0.25, and from 4.40 Å to 4.41 Å at a molar ratio R of 0.5). These values are similar to those of the stable conformers of the methyl-esterified galacturonate disaccharide identified by Cros et al. using molecular mechanics calculations (h = 4.3–4.4 Å) (Cros et al., 1992). They also lie between those computed by Braccini et al. for regular GalA helices in the 2_1 (h = 4.25 Å) and in the 3_1 conformations (h = 4.43 Å), respectively, from adiabatic maps of digalacturonic acid (Braccini et al., 1999). Therefore, the present MD simulations suggest that the partial methyl-esterification of PGA chains has a rather limited effect on the helix raise h. In contrast, it induces a significant shift of the probability distribution of the helix turn angle θ toward smaller values (Fig. 6 and Fig. S8 in the Supporting Information), which corresponds to an increase of the population of the 3_1 helical conformation (from 37–44 % to 48–58 %) and, concomitantly, to a decrease of that of the 2_1 helical conformation (from 46–57 % to 37–47 %, see Table S4 and Fig. S9 in the Supporting Information). Given that the egg-box model (EBM) (Grant, Morris, Rees, Smith, & Thom, 1973) hypothesizes a two-fold 2_1 helix conformation of PGA chains in junction zones, this result suggests that the partial methyl-esterification of PGA chains favors the formation of junction zones with geometries that deviate from that hypothesized in the EBM. Moreover, Fig. 6 and Table S4 evidence that GalA chains sample more frequently the 3_1 helical conformation when the concentration of calcium cations increases, for both DM and GalA concentrations considered, thereby corroborating the remark of Perez and coworkers, who anticipated that intermolecular interactions with neighboring ions, solvent, and other macromolecules may easily induce a conformational change (Pérez et al., 2000). It must also be noted that such conformational changes induced by methyl-esterification and/or the presence of calcium at molar ratios of 0.25 and 0.5 appear as an enhanced sampling of the (ϕ,ψ) glycosidic angles region with ψ angles lower than 60° in the free energy maps, ΔF(ϕ,ψ) (see Fig. S10 in the Supporting Information), whose minima seem in line with that of the (ϕ,ψ) contour plot determined by Alba et al. for a GalA decamer with a DM of 10 % at pH 7.(Alba et al., 2018) In addition, the conformational freedom of PGA chains suggested by Fig. 6 and Table S4 in the Supporting Information is in line with the ^{13}C NMR study of Jarvis and Apperley on concentrated Ca-PGA gels, which showed that PGA chains are primarily in the 2_1 helix conformation, but that they also substantially sample 3_1 and intermediate helix conformations (Jarvis & Apperley, 1995). Such conformational disorder also appears consistent with the existence of several stable conformers for the methyl-esterified galacturonate disaccharide found in ref. (Cros et al., 1992).

3.5.2. Chain association

We then studied the effect of methyl-esterification on the association of PGA chains. To this aim, we first calculated several intermolecular radial distribution functions, g(r), between the carboxylate carbon atoms, C_{carb}, of PGA chains (Fig. 7a and Fig. S11a-d in the Supporting Information), between the methyl carbon atoms, C_M, of methyl-esterified PGA chains (Figs. 7b and S11e-f in the Supporting Information), and between the carboxylate carbon atoms of PGA chains and calcium cations (Fig. 7c). The $g_{C_{carb}-C_{carb}}(r)$ distributions show a strong exclusion of PGA chains from one another at $R = 0.0$, which stems from the strong electrostatic repulsion between these highly negatively charged chains ($q_{PGA} = -16$ e for DM = 0 % and $q_{PGA} = -11$ e for DM = 31 %), in spite of the presence of sodium counterions. As expected, the

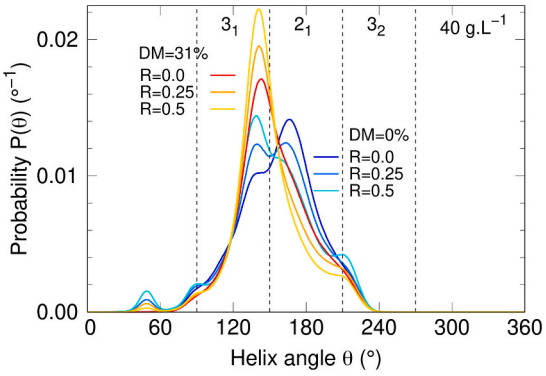

Fig. 6. Normalized probability distribution, P(θ), of the dihedral angle θ describing the helicity of PGA chains at a [GalA] concentration of 40 g.L^{-1}, with DM of 0 % and 31 % and [Ca^{2+}]/[GalA] molar ratios, R, of 0.0, 0.25 and 0.5. The corresponding distributions at a [GalA] concentration of 20 g.L^{-1} are shown in Fig. S8 in the Supporting Information.

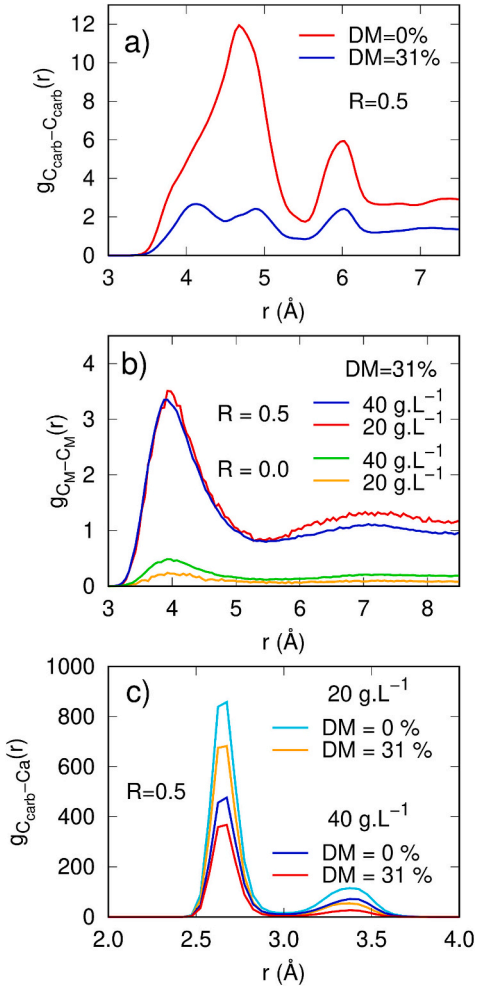

Fig. 7. Intermolecular radial distribution functions, g(r), between carboxylate carbon atoms at $R = 0.50$ and [GA] = 40 g.L^{-1} (a), between methyl carbon atoms at [GA] of 20 g.L^{-1} and 40 g.L^{-1} (b), and between carboxylate carbon atoms and calcium cations at R = 0.50 (c). The $g_{C_{carb}-C_{carb}}(r)$ (both at 20 and 40 g.L^{-1}) and $g_{C_M-C_M}(r)$ radial distribution functions are shown up to distances of 45 Å in Fig. S11 in the Supporting Information.

chain-chain exclusion is slightly more pronounced for DM = 0 % owing to the more negatively charged chains. In the presence of calcium at molar ratios R of 0.25 and 0.5, striking changes in the intermolecular $g_{C_{carb}-C_{carb}}(r)$ distributions are observed. In particular, sharp peaks at distances below 7.5 Å emerge. These peaks originate from the formation of GalA-Ca^{2+}-GalA cross-links between PGA chains. Moreover, two broader peaks are observed at distances of about 11 Å and 16 Å and correspond to the C_{Carb} atoms from the first and the second GalA neighbors from the GalA units involved in a given cross-link, since the average pitch distance is close to 4.4 Å (Fig. S7 in the Supporting Information). Figs. 7a and S11a-d indicate that methyl-esterification of PGA chains decreases the number of cross-links formed, particularly at a concentration of 40 g.L^{-1} and a molar ratio of 0.5. Furthermore, the presence of several peaks clearly illustrates the diversity of geometries of the cross-links formed, as opposed to the one peak located at the distance of about 6.8 Å, which would correspond to the monodentate coordination of calcium cation to the carboxylate carbon atom from two associated chains, as suggested by the EBM. The changes observed in the positions and intensities of the peaks found at distances below 7.5 Å are not straightforward to interpret. In order to relate these peaks to local cross-links geometries, we determined the probability distributions of the three distances (called d_1, d_2, and d_3) and the three angles (called a_1, a_2, and a_3) describing the GalA-Ca^{2+}-GalA cross-links (see Figs. S12, S13, and S14 in the Supporting Information for further details). The two C_{carb}-Ca^{2+} distance probability distributions, $P(d_1)$ and $P(d_2)$, exhibit two peaks at distances close to 2.7 Å and 3.4 Å, which represent bidentate and monodentate contact ion pairs (CIP) between calcium and GalA units, respectively (Assifaoui et al., 2015; Huynh et al., 2016; Lerbret & Assifaoui, 2022) and which correspond to the two peaks of the $g_{C_{carb}-Ca^{2+}}(r)$ distributions shown in Fig. 7c. The larger peak of the bidentate CIP is consistent with the preferential coordination of calcium in a bidentate coordination to the carboxylate group of GalA and guluronic (GulA) units observed in previous MD studies of polyuronates in the presence of calcium (Assifaoui et al., 2015; Fu et al., 2014; Huynh et al., 2016; Lerbret & Assifaoui, 2022; Li et al., 2021; Plazinski, 2011; Wolnik et al., 2013).

The analysis of distance and angle distributions describing cross-links then allowed us to ascribe the sharp peaks of the $g_{C_{carb}-C_{carb}}(r)$ distributions to the following coordination modes (see section *Geometry of cross-links* in the Supporting Information): bidentate-bidentate (r ≈ 4.1 Å), bidentate-bidentate and bidentate-monodentate (r ≈ 4.9 Å); bidentate-bidentate and bidentate-monodentate (r ≈ 5.4 Å); bidentate-monodentate and monodentate-monodentate (r ≈ 6.0 Å); monodentate-monodentate (r ≈ 6.7 Å). Interestingly, the probability distributions of the a_1, a_2, and a_3 angles indicate that the cross-links formed between partially methyl-esterified PGA chains are slightly more distorted (Figs. S13d-f and S14d-f), except at a ratio R of 0.5 and a GalA concentration of 40 g.L^{-1}, and, thus, probably less stable, than those formed between non-methyl-esterified PGA chains. Nevertheless, it must be pointed out that the association between partially methyl-esterified PGA chains may be stabilized by hydrophobic contacts between the methyl groups of methyl-esterified GalA units, which are revealed by the peak located at a distance r of 3.9–4.0 Å in the $g_{C_M-C_M}(r)$ distributions, whose height strongly increases when R increases from 0 to 0.5 (Figs. 7b and S11e-f in the Supporting Information). In the absence of calcium ($R = 0.0$), these hydrophobic interactions are clearly overwhelmed by the strong repulsive electrostatic repulsion between PGA chains.

For an easier quantitative comparison of the effect of partial methyl-esterification on the association of PGA chains induced by the presence of calcium at molar ratios R of 0.25 and 0.5, we also determined (i) the number of calcium cations bound to PGA chains (DP = 16, ~2820 g/mol), NB, (ii) the number of cross-links formed between PGA chains, NC, and (iii) the number of contacts between the methyl groups of partially methyl-esterified PGA chains, NM (see Figs. 8a and S16 in the Supporting Information). Almost all calcium cations (between 92 % and 97 % depending on the [GalA] and DM considered) are bound to PGA chains at a molar ratio R of 0.25, in agreement with the high affinity between calcium and GalA units revealed by the $g_{C_{carb}-Ca}(r)$ radial distributions (Fig. 7c). However, the number of bound calcium cations are lower for partially methyl-esterified PGA chains than for non-methyl-esterified chains at a molar ratio of 0.5 (75–80 % vs. 92–96 %, respectively, depending on the GalA concentration considered, see Fig. S16a-b in the Supporting Information). Such difference may be explained by the molar ratios needed to neutralize the total negative charge of PGA chains, which are of 0.5 and 0.34 for DM = 0 % and DM = 31 %, respectively, if we assume that the binding of Ca^{2+} to PGA chains with an effective neutral (or positive) charge would be less favorable. Moreover, at a molar ratio R of 0.25, the ratio of NC to the number of GalA units, N_{GalA}, remains lower (between 0.04 and 0.10) than the one expected in the junction zones of dimers according to the EBM (0.25). This ratio increases significantly for non-methyl-esterified PGA chains when R increases up to 0.5 ($NC/N_{GalA} = 0.17$ and 0.26, for GalA concentrations of 20 g.L^{-1} and 40 g.L^{-1}, respectively). It must be pointed out that according to the EBM, NC/N_{GalA} ranges from 0.25 for a dimer to (n-1)/(2n) for a n-mer, which leads to 0.5 if n is infinite. Similarly, if we extend the EBM to PGA chains in the 3_1 helical conformation, then NC/N_{GalA} would range from 1/6 for a dimer to (n-1)/(3n) for a n-mer, which

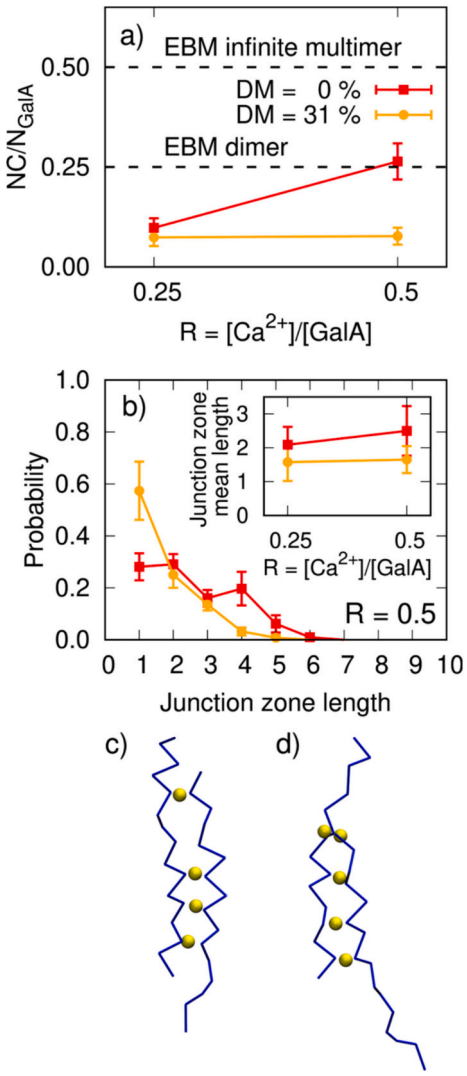

Fig. 8. (a) Ratio of the number of cross-links, NC, to the number of GalA units in the simulation boxes, N_{GalA}, as a function of the $[Ca^{2+}]$/[GalA] molar ratio, R, and at a concentration [GalA] of 40 g.L^{-1}. The values of 0.25 and 0.5 hypothesized for the junction zones in an ideal EBM dimer and in an infinite EBM multimer, respectively, are shown for comparison as horizontal dashed lines. (b) Probability distribution of the size of junction zones formed between pairs of PGA chains at a molar ratio R of 0.5 for DM = 0 % and DM = 31 %, at a concentration [GalA] of 40 g.L^{-1}. The inset shows the corresponding mean size of junction zones determined from these distributions. Two cross-links between a pair of PGA chains were considered to be neighbors from one another and, therefore, to belong to a given junction zone, if the minimal distance along PGA chains between the GalA units involved in the cross-links was lower or equal to 2 (in number of GalA units). Point-like cross-links were considered as junction zones of size 1. Examples of pairs of cross-linked PGA chains (DM = 0 %) with junction zones of sizes 1 and 3 and of size 4 are shown in (c) and (d), respectively. For clarity, only the calcium cations involved in cross-links between the two chains are displayed. Moreover, other PGA chains from the simulation box are not shown.

would lead to 1/3 if n is infinite. To further characterize the distribution of the cross-links formed between pairs of PGA chains in the presence of calcium, we then determined the probability distribution of the size of junction zones (Fig. 8b and Fig. 17a-d in the Supporting Information). The distributions are clearly shifted toward lower sizes for PGA chains with DM = 31 %, which can be ascribed to the presence of methylesterified GalA units, which cannot be involved in cross-links. Nonetheless, these results also evidence that rather short junction zones (with sizes of 2, 3, and 4 cross-links) are formed even for PGA chains with DM = 0 %, so that the mean size of junction zones does not exceed 2.5 ± 0.7 cross-links for the most cross-linked system investigated ([GalA] = 40 g.L^{-1} and DM = 0 %, see inset of Figs. 8b and S17e-f in the Supporting Information), whereas junction zones composed of 8 cross-links could be formed with hexadecameric GalA chains according to the EBM. Two examples of pairs of PGA chains with DM = 0 % cross-linked with junction zones of size 1, 3, and 4 are displayed in Fig. 8c-d. These results suggest that significant defects exist in the cross-linking patterns of associated PGA and MeO-PGA chains. However, shorter junctions will lead to lower mechanical strength of the calcium PGA gel, compared to a gel in which longer junctions can be obtained, as the reduced Young moduli of Ca-MeO-PGA gels suggest (Fig. 4b) and shown for different types of pectin (Ström et al., 2007). A calcium pectin gel derived from pectin with a randomly distributed methyl ester pattern, and thus statistically shorter junctions, is considerably weaker than a calcium pectin gel formed from a pectin with a blockwise distribution of methyl ester patterns, where longer junctions are statistically probable, regardless of DM (Ström et al., 2007). The results presented from the MD simulations indicate the presence of significant amounts (25–41 % when DM = 0 % and 43–59 % when DM = 31 %) of isolated, point-like cross-links (that is, junction zones of size 1), in line with our previous MD study on the association between calcium and octameric GalA chains, which showed that bound calcium may be found both in monocomplexes, point-like cross-links, and highly cross-linked complexes ($N_C/N_{GalA} \geq 0.125$) at a molar ratio R of 0.25 (Lerbret & Assifaoui, 2022). The simulation results are thus pointing toward mostly short junction zones (<4 GalA units). However, the simulated systems differ from experimental ones in many respects (short length of PGA chains – DP = 16 – and short simulation times, absence of mechanical loading), which may result in an overestimation of short junction zones. It should also be noted that the association behavior of PGA chains likely depends on their length, and that the simulated PGA chains (DP = 16) might be too short to experience the cooperative binding of calcium observed experimentally, so that the population of point-like cross-links is likely overestimated in MD simulations, but also, it does not take into account whether or not the junction is load bearing, nor rearrangement to more favorable positions over time. The number of contacts between methylester groups (hydrophobic interactions), NM, is found between about 11 to 21 times lower than NC, depending on the GalA concentration and the molar ratio R considered, which suggests that the binding of calcium to GalA units remains by far the main driving force for the ionotropic gelation of partially methyl-esterified PGA chains.

4. Discussion

Gels formed by the diffusion of divalent ions from an external reservoir to a polyuronate solution (pectins, alginates) exhibit heterogeneity with significant concentration gradients in both the polymer and the divalent cation concentrations (Caccavo et al., 2016; Maire du Poset et al., 2018; Maire du Poset et al., 2019; Skjåk-Bræk et al., 1989; Thu et al., 2000). Calcium-PGA gels are fully transparent and show no mesoscopic heterogeneities across the gel network (Fig. 3). In the regions of the hydrogel formed in the early stage of gelation (near parts), a high polymer concentration of 35 g.L^{-1} (Fig. 4a) leads to a strong elastic modulus (Fig. 4b) as demonstrated in our previous work (Maire du Poset et al., 2018). Conversely, regions formed in later stages (far parts) have a lower polymer concentration (9 g.L^{-1}), resulting in a less rigid gel structure. The ratio between these two concentrations in slice 1 (near) and slice 4 (far) C_{Near}/C_{Far} is about 4. The mesh size in the nearest regions, measured by SANS, is approximately 75 Å, which is remarkably close to the persistence length (Lp) of PGA. This mesh size indicates that the network contraction is limited by the persistence length, as the chains cannot compress further (Maire du Poset et al., 2018; Maire du Poset et al., 2019). In the furthest regions, the local structure remains homogeneous, but with an increased mesh size to accommodate the reduced PGA concentration as described in Fig. 9 (Maire du Poset et al.,

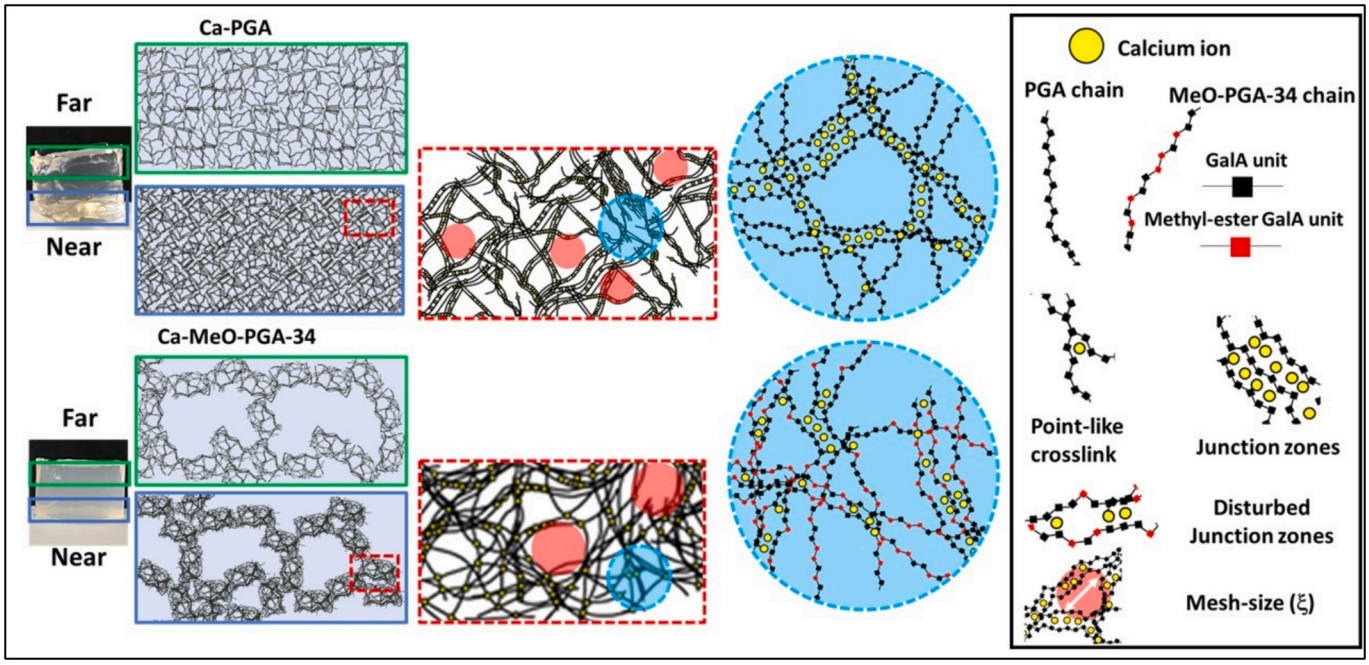

Fig. 9. Schematic representation of the mesoscopic and local structures of the Ca-PGA and Ca-MeO-PGA-34 gels.

2019; Maire du Poset, Börjesson, et al., 2020).

Gelation of methyl-esterified PGA through calcium diffusion produced more turbid gels (Fig. 3). In Fig. 9, we present a comparison of the local structure of Ca-MeO-PGA-34 to that of Ca-PGA. In the Ca-MeO-PGA-34 hydrogel, the polymer concentration gradient is less pronounced than in the Ca-PGA one (Fig. 4a). For this sample, the polymer concentration gradient actually decreases from 30 $g.L^{-1}$ in the Near region to 15 $g.L^{-1}$ in the Far region of the gel, corresponding to a C_{Near}/C_{Far} ratio close to 2. The polymer concentration gradient within the methylated gel is much less pronounced than in the non-methylated gel, which originates from the fact that the methylated PGA chains have a lower lineic charge density. Indeed, when Ca^{2+} cations diffuse into the transient network of the PGA, their complexation gradually reduces the charge density of these chains, which locally raises the chemical potential of water molecules. This creates a gradient of chemical potential between the complexed (Near) part of the gel and the non-complexed part of the solution. This water hydration migration is responsible for the formation of the gradient, that is as large as the nominal charge density of the chains is important (Huynh, Chambin, Maire du Poset, & Assifaoui, 2018). SANS measurements for slice 1 (Near region) reveal an increased mesh size of approximately 140 Å, exceeding the persistence length (Lp) of Ca-MeO-PGA-34 chains (Lp = 84 Å). This larger mesh size can be attributed to the methyl-esterification of PGA, which reduces the number of negatively charged groups along the chains. Accordingly, partially methyl-esterified PGA chains are less prone to self-associate than non-methylated PGA chains in the presence of calcium at a [Ca]/[GalA] molar ratio of 0.5, as shown by Figs. 7a and 8a. Furthermore, methylation promotes the formation of 3_1 conformations over the regular 2_1 conformations observed predominantly in PGA, making MeO-PGA-34 stiffer than PGA (Fig. 6 and Figs. S8 and S9 and Table S4 in the Supporting Information). For Ca-PGA, the associations between GalA chains and Ca^{2+} involve both point-like crosslinks as well as numerous dimers and multimers, resulting in a uniform network structure throughout the gel (Fig. 9). In contrast, for Ca-MeO-PGA-34, the formation of point-like crosslinks is more prevalent, while structured dimers and multimers are less readily formed. Fig. 8b indeed reveals that, in the MD simulations, point-like cross-links represent about 57 ± 11 % of all the cross-links formed between pairs of methylated PGA chains (DM = 31 %) at a concentration of 40 $g.L^{-1}$ and a molar ratio R of 0.5, while short junction zones composed of 2 and 3 cross-links account for only 25 ± 5 % and 14 ± 2 % of the cross-links formed, respectively. This organization likely induces local structural heterogeneity that may diffuse throughout the gel, preventing chain compaction to match the persistence length (Lp). However, to achieve the large porosity responsible for the visible turbidity, a dense polymer chain network is required (Fig. 9).

5. Conclusion

This study showed how the partial methyl-esterification of PGA chains modulates the anisotropy of Ca-PGA hydrogels. It induces turbidity in Ca-PGA hydrogels, which reflects the emergence of heterogeneities of mesoscopic sizes, increases their mesh size, and reduces the gradients in PGA and calcium concentrations. Small-angle neutron scattering (SANS) analysis shows that methylation increases the persistence length (Lp) of PGA chains, while molecular dynamics (MD) simulations reveal a stabilization of 3_1 helical conformations. This increased chain rigidity weakens the affinity of PGA for calcium cations and reduces the extent of chain–chain cross-linking. Such results likely stem from the presence of methyl-ester groups, which hinder the formation of junction zones between PGA chains and lower their negative charge. Moreover, MD simulations on PGA chains (DP = 16) showed that binding is primarily governed by bridging interactions with carboxylate groups in the bidentate mode. In contrast, hydrophobic interactions are significantly less frequent (about 11 to 21 times lower). Yet, it should be noted that it is not straightforward to unambiguously disentangle the impact of methylation from that of the molar mass of PGA chains, M_w, given that M_w systematically decreases when DM increases following the methyl-esterification reaction employed. Nonetheless, this study suggests that the partial methylation of PGA chains represents a promising method to tune the diffusion of encapsulated drugs, which depends on their relative size with respect to the mesh size of the polymer network, as well as the mechanical strength of hydrogels, which decreases with their density of cross-links.

CRediT authorship contribution statement

Mikaela Börjesson: Writing – original draft, Project administration,

Investigation, Formal analysis, Conceptualization. **Giovanni Tizzanini:** Writing – review & editing, Methodology. **Anna Ström:** Writing – review & editing, Supervision, Methodology. **Adrien Lerbret:** Writing – review & editing, Writing – original draft, Methodology, Formal analysis. **Fabrice Cousin:** Writing – review & editing, Writing – original draft, Validation, Supervision, Funding acquisition, Conceptualization. **Ali Assifaoui:** Writing – review & editing, Writing – original draft, Supervision, Methodology, Funding acquisition, Conceptualization.

Funding sources

Any funds used to support the research of the manuscript should be placed here (per journal style).

Declaration of competing interest

The authors declare the following financial interests/personal relationships which may be considered as potential competing interests: Assifaoui reports financial support and article publishing charges were provided by University of Burgundy. If there are other authors, they declare that they have no known competing financial interests or personal relationships that could have appeared to influence the work reported in this paper.

Acknowledgments

This project was funded under the Nordic Neutron Science Programme “ NNSP International Post Doc fellowships” N°87791 (2018 – 2020). This project was provided with computing HPC and storage resources by GENCI at TGCC thanks to the grants 2021-A0110707745 and 2022-A0130707745 on the supercomputer Joliot Curie’s ROME partition, at IDRIS thanks to the grant 2023-A0150813818 on the supercomputer Jean Zay’s CSL partition, and at CINES thanks to the grant 2024-A0170714657 on the supercomputer Adastra’s GENOA partition. Some simulations were also performed using HPC resources from DNUM-CCUB (Université Bourgogne Europe). We also acknowledge financial contribution from Swedish Research Council, FORMAS grant number 2020-02843.

Appendix A. Supplementary data

The Supporting Information is available free of charge. Gelation protocol; NMR spectra for PGA and MeO-PGA solutions; Flow behavior of PGA and MeO-PGA solutions; SANS spectra of PGA solutions at a concentration of 20 $g.L^{-1}$; Persistence length of PGA chains determined from SANS spectra; Molar ratio [Ca]/[GalA] as a function of the gel slice; Calcium and PGA contents in gel slices; SANS spectra of gel slices; MD simulations details; Helical parameters of PGA chains; Populations of the helical conformations of PGA chains; Free-energy maps, ΔF, in the subspace of the glycosidic dihedral angles, Φ and Ψ; Intermolecular radial distribution functions between carboxylate carbon atoms and between methyl carbon atoms; Distance and angle distributions of cross-links; Numbers of bound calcium cations, cross-links, and methyl contacts; Size distributions of junction zones. Supplementary data to this article can be found online at https://doi.org/10.1016/j.carbpol.2025.124301.

Data availability

Data will be made available on request.

References

Abraham, M. J., Murtola, T., Schulz, R., Páll, S., Smith, J. C., Hess, B., & Lindahl, E. (2015). GROMACS: high performance molecular simulations through multi-level parallelism from laptops to supercomputers. *SoftwareX, 1-2*, 19–25.

Alba, K., Bingham, R. J., Gunning, P. A., Wilde, P. J., & Kontogiorgos, V. (2018). Pectin conformation in solution. *The Journal of Physical Chemistry B, 122*(29), 7286–7294.

Alba, K., Bingham, R. J., & Kontogiorgos, V. (2017). Mesoscopic structure of pectin in solution. *Biopolymers, 107*(6), Article e23016.

Assifaoui, A., Hayrapetyan, G., Gallery, C., & Agoda-Tandjawa, G. (2024). Exploring techno-functional properties, synergies, and challenges of pectins: A review. *Carbohydrate Polymer Technologies and Applications, 7*, Article 100496.

Assifaoui, A., Lerbret, A., Uyen, H. T. D., Neiers, F., Chambin, O., Loupiac, C., & Cousin, F. (2015). Structural behaviour differences in low methoxy pectin solutions in the presence of divalent cations (Ca^{2+} and Zn^{2+}): A process driven by the binding mechanism of the cation with the galacturonate unit. *Soft Matter, 11*(3), 551–560.

Braccini, I., Grasso, R. P., & Pérez, S. (1999). Conformational and configurational features of acidic polysaccharides and their interactions with calcium ions: A molecular modeling investigation. *Carbohydrate Research, 317*(1–4), 119–130.

Caccavo, D., Ström, A., Larsson, A., & Lamberti, G. (2016). Modeling capillary formation in calcium and copper alginate gels. *Materials Science and Engineering: C, 58*, 442–449.

Cao, L., Lu, W., Mata, A., Nishinari, K., & Fang, Y. (2020). Egg-box model-based gelation of alginate and pectin: A review. *Carbohydrate Polymers, 242*, Article 116389.

Chen, J., Liu, W., Liu, C. M., Li, T., Liang, R. H., & Luo, S. J. (2015). Pectin modifications: A review. *Critical Reviews in Food Science and Nutrition, 55*(12), 1684–1698.

Cros, S., du Penhoat, C. H., Bouchemal, N., Ohassan, H., Imberty, A., & Pérez, S. (1992). Solution conformation of a pectin fragment disaccharide using molecular modelling and nuclear magnetic resonance. *International Journal of Biological Macromolecules, 14*(6), 313–320.

Fu, H., Liu, Y., Adrià, F., Shao, X., Cai, W., & Chipot, C. (2014). From material science to Avant-Garde cuisine. The art of shaping liquids into spheres. *The Journal of Physical Chemistry. B, 118*(40), 11747–11756.

Grant, G. T., Morris, E. R., Rees, D. A., Smith, P. J. C., & Thom, D. (1973). Biological interactions between polysaccharides and divalent cations: The egg-box model. *FEBS Letters, 32*, 195–198.

Huynh, U. T. D., Chambin, O., Maire du Poset, A., & Assifaoui, A. (2018). Insights into gelation kinetics and gel front migration in cation-induced polysaccharide hydrogels by viscoelastic and turbidity measurements: Effect of the nature of divalent cations. *Carbohydrate Polymers, 190*, 121–128.

Huynh, U. T. D., Lerbret, A., Neiers, F., Chambin, O., & Assifaoui, A. (2016). Binding of divalent cations to polygalacturonate: A mechanism driven by the hydration water. *The Journal of Physical Chemistry. B, 120*(5), 1021–1032.

Jangizehi, A., Schmid, F., Besenius, P., Kremer, K., & Seiffert, S. (2020). Defects and defect engineering in soft matter. *Soft Matter, 16*(48), 10809–10859.

Jarvis, M. C., & Apperley, D. C. (1995). Chain conformation in concentrated pectic gels: Evidence from ^{13}C NMR. *Carbohydrate Research, 275*(1), 131–145.

Kpodo, F. M., Agbenorhevi, J. K., Alba, K., Bingham, R. J., Oduro, I. N., Morris, G. A., & Kontogiorgos, V. (2017). Pectin isolation and characterization from six okra genotypes. *Food Hydrocolloids, 72*, 323–330.

Lerbret, A., & Assifaoui, A. (2022). How accurate is the egg-box model in describing the binding of calcium to polygalacturonate? A molecular dynamics simulation study. *The Journal of Physical Chemistry. B, 126*(48), 10206–10220.

Li, J., & Mooney, D. J. (2016). Designing hydrogels for controlled drug delivery. *Nature Reviews Materials, 1*, Article 16071.

Li, X., & Su, X. (2018). Multifunctional smart hydrogels: Potential in tissue engineering and cancer therapy. *Journal of Materials Chemistry B, 6*, 4714–4730.

Li, Z. J., Srebnik, S., & Rojas, O. J. (2021). Revisiting cation complexation and hydrogen bonding of single-chain polyguluronate alginate. *Biomacromolecules, 22*(9), 4027–4036.

Maire du Poset, A., Börjesson, M., Rameau, C., Madeleine-Perdrillat, C., Lerbret, A., Loupiac, C., … Assifaoui, A. (2020). Controlled loading and release of beta-lactoglobulin in calcium-polygalacturonate hydrogels. *Biomacromolecules, 21*(4), 1417–1426.

Maire du Poset, A., Lerbret, A., Boué, F., Zitolo, A., Assifaoui, A., & Cousin, F. (2019). Tuning the structure of galacturonate hydrogels: External gelation by Ca, Zn, or Fe cationic cross-linkers. *Biomacromolecules, 20*(7), 2864–2872.

Maire du Poset, A., Lerbret, A., Zitolo, A., Cousin, F., & Assifaoui, A. (2018). Design of polygalacturonate hydrogels using iron(II) as cross-linkers: A promising route to protect bioavailable iron against oxidation. *Carbohydrate Polymers, 188*, 276–283.

Maire du Poset, A., Zitolo, A., Cousin, F., Assifaoui, A., & Lerbret, A. (2020). Evidence for an egg-box-like structure in iron(ii)–polygalacturonate hydrogels: A combinedEXAFS and molecular dynamics simulation study. *Physical Chemistry Chemical Physics, 22*, 22–2977..

Maki, Y., Ito, K., Hosoya, N., Yoneyama, C., Furusawa, K., Yamamoto, T., Dobashi, T., Sugimoto, Y., & Wakabayashi, K. (2011). Anisotropic structure of calcium-induced alginate gels by optical and small-angle X-ray scattering measurements. *Biomacromolecules, 12*(6), 2145–2152.

Matsumoto, Y., Shundo, A., Ohno, M., Tsuruzoe, N., Goto, M., & Tanaka, K. (2017). Evolution of heterogeneity accompanying sol–gel transitions in a supramolecular hydrogel. *Soft Matter, 13*(40), 7433–7440.

Mørch, Ý. A., Donati, I., & Strand, B. L. (2006). Effect of Ca^{2+}, Ba^{2+}, and Sr^{2+} on alginate microbeads. *Biomacromolecules, 7*(5), 1471–1480.

Müller-Maatsch, J., Caligiani, A., Tedeschi, T., Elst, K., & Sforza, S. (2014). Simple and validated quantitative ^{1}H NMR method for the determination of methylation, acetylation, and feruloylation degree of pectin. *Journal of Agricultural and Food Chemistry, 62*(37), 9081–9087.

Nicolella, P., Koziol, M. F., Löser, L., Saalwächter, K., Ahmadi, M., & Seiffert, S. (2022). Defect-controlled softness, diffusive permeability, and mesh-topology of metallo-supramolecular hydrogels. *Soft Matter, 18*(5), 1071–1081.

Pérez, S., Mazeau, K., & Hervé du Penhoat, C. (2000). The three-dimensional structures of the pectic polysaccharides. *Plant Physiology and Biochemistry, 38*(1–2), 37–55.
Perić, L., Pereira, C. S., Pérez, S., & Hünenberger, P. H. (2008). Conformation, dynamics and ion-binding properties of single-chain polyuronates: A molecular dynamics study. *Molecular Simulation, 34*(4), 421–446.
Plazinski, W. (2011). Molecular basis of calcium binding by polyguluronate chains. Revising the egg-box model. *Journal of Computational Chemistry, 32*(14), 2988–2995.
Rehmann, M. S., Skeens, K. M., Kharkar, P. M., Ford, E. M., Maverakis, E., Lee, K. H., & Kloxin, A. M. (2017). Tuning and predicting mesh size and protein release from step growth hydrogels. *Biomacromolecules, 18*(10), 3131–3142.
Rose, K. A., Marino, E., O'Bryan, C. S., Murray, C. B., Lee, D., & Composto, R. J. (2022). Nanoparticle dynamics in hydrogel networks with controlled defects. *Soft Matter, 18*(47), 9045–9056.
Rosenbohm, C., Lundt, I., Christensen, T. M. I. E., & Young, N. W. G. (2003). Chemically methylated and reduced pectins: Preparation, characterisation by ^{1}H NMR spectroscopy, enzymatic degradation, and gelling properties. *Carbohydrate Research, 338*(7), 637–649.
Schuster, E., Eckardt, J., Hermansson, A.-M., Larsson, A., Lorén, N., Altskär, A., & Ström, A. (2013). Microstructural, mechanical and mass transport properties of isotropic and capillary alginate gels. *Soft Matter, 10*, 357–366.
Schuster, E., Sott, K., Ström, A., Altskär, A., Smisdom, N., Gebäck, T., Lorén, N., & Hermansson, A.-M. (2016). Interplay between flow and diffusion in capillary alginate hydrogels. *Soft Matter, 12*(17), 3897–3907.
Skjåk-Bræk, G., Grasdalen, H., & Smidsrød, O. (1989). Inhomogeneous polysaccharide ionic gels. *Carbohydrate Polymers, 10*(1), 31–54.
Ström, A., Ribelles, P., Lundin, L., Norton, I., Morris, E. R., & Williams, M. A. K. (2007). Influence of pectin fine structure on the mechanical properties of calcium-pectin and acid-pectin gels. *Biomacromolecules, 8*(9), 2668–2674.
Thiele, H., & Hallich, K. (1957). Kapillarstrukturen in ionotropen Gelen. *Kolloid-Zeitschrift, 151*(1), 1–12.
Thu, B., Gåserød, O., Paus, D., Mikkelsen, A., Skjåk-Bræk, G., Toffanin, R., Vittur, F., & Rizzo, R. (2000). Inhomogeneous alginate gel spheres: An assessment of the polymer gradients by synchrotron radiation-induced x-ray emission, magnetic resonance microimaging, and mathematical modeling. *Biopolymers, 53*(1), 60–71.
Van Der Spoel, D., Lindahl, E., Hess, B., Groenhof, G., Mark, A. E., & Berendsen, H. J. C. (2005). GROMACS: Fast, flexible, and free. *Journal of Computational Chemistry, 26*(16), 1701–1718.
Wolnik, A., Albertin, L., Charlier, L., & Mazeau, K. (2013). Probing the helical forms of Ca^{2+}–guluronan junction zones in alginate gels by molecular dynamics 1: Duplexes. *Biopolymers, 99*(8), 562–571.
Wu, Z. L., Kurokawa, T., Sawada, D., Hu, J., Furukawa, H., & Gong, J. P. (2011). Anisotropic hydrogel from complexation-driven reorientation of semirigid polyanion at Ca^{2+} diffusion flux front. *Macromolecules, 44*(9), 3535–3541.
Wu, Z. L., Takahashi, R., Sawada, D., Arifuzzaman, M., Nakajima, T., Kurokawa, T., … Gong, J. P. (2014). In situ observation of Ca^{2+} diffusion-induced superstructure formation of a rigid polyanion. *Macromolecules, 47*(20), 7208–7214.